ORIGINAL PAPER

Journal of Textile Engineering (2008), Vol.54, No.2, 41 - 47

Geometry Effect of Air Suction Gun on the Yarn Suction Characteristics

IEMOTO Yoshiyuki[a,*], TANOUE Shuichi[a], HOSOKAWA Jun-ichi[a], LI Yonggui[a],
MASUDA Atsuji[b], MURAKAMI Tetsuhiko[b]

[a] *Graduate School of Engineering, University of Fukui, Bunkyo, Fukui 910–8507, Japan*
[b] *Industrial Technology Center of Fukui Prefecture, 61-10 Kawaiwashizuka-cho, Fukui 910–0102, Japan*

Received 16 December 2007; accepted for publication 11 April 2008

Abstract

We experimentally discussed the effects of airflow geometries in an air suction gun on the suction characteristics of running yarn. Geometry parameters focused on were 1) compressed-air inflow angle of nozzle, 2) diverging angle of nozzle, 3) throat diameter of de Laval tube, 4) converging angle of de Laval tube and 5) yarn propulsion tube length. As a result, effects of the geometry parameters on the yarn suction force, the mass flow rate of compressed-air and the yarn suction efficiency, which is defined as the yarn suction force divided by the mass flow rate of compressed-air, were made clear and the optimum geometry of an air suction gun was obtained on the basis of the energy efficiency. In addition, the yarn suction force showed two types of time dependency because of different yarn motion on some experimental conditions.

Key Words: Suction gun, Geometry effect, Yarn suction force, Yarn suction efficiency, Fluid machinery

1. Introduction

An air suction gun is a kind of fluid machinery that sucks one or more running yarns by both injector mechanism and friction of a high-speed air. It is used for taking the running yarn to a winder at the beginning of yarn making and processing. Figure 1 shows a typical air suction gun. The compressed air enters the air suction gun through the lower part ① as shown in Fig. 1(a) and jets from the compressed-air inflow tubes ② to the yarn channel of the nozzle. The detail of the nozzle is shown in Fig. 1(b). The axes of four compressed-air inflow tubes have the circumferential and axial components of the yarn channel of the nozzle. The compressed air issued from the compressed-air inflow tubes expands, passes spirally through the yarn propulsion tube, which is composed of the de Laval tube and the straight tube, and flows out from the exit ③ of the air suction gun. The running yarn sucked from the entrance ④ of the yarn inhalation tube is given a high propulsion in the yarn propulsion tube by the air issued from the compressed-air inflow tubes and blown out from the exit ③ of the air suction gun together with the air issued from the compressed-air inflow tubes.

The required performance of an air suction gun is 1) powerful suction of yarn, 2) low consumption of air, 3) compact size, 4) low noise and so on. Since the air suction gun is one of

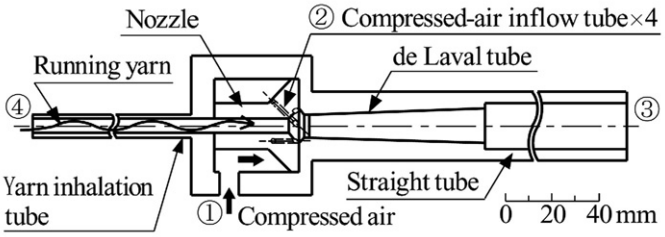

(a) Whole

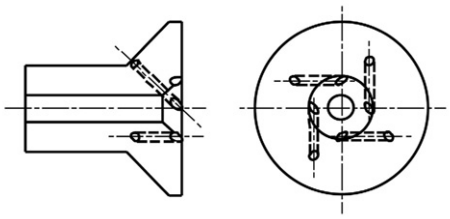

(b) Nozzle

Fig. 1 Illustration of a typical air suction gun.

fluid machinery using compressed air, the airflow geometry in the air suction gun would obviously have some effects on its performance. In this study, we focused on the geometry of an air suction gun, thus we studied experimentally the geometry effects of an air suction gun on the yarn suction characteristics, which is one of the evaluation values of the performance of an air suction gun.

In the textile machinery subjects, there are many kinds of

* Corresponding author: E-mail: iemoto@matse.fukui-u.ac.jp, Tel: +81-776-27-8625, Fax: +81-776-27-8767

fluid machinery using an airflow, e.g. an interlacer in the interlacing process [1–15], an air-jet loom in the weaving process [16–19], etc. And the basic studies of these subjects were carried out actively by several researchers. However, there is little literature of the study of the air suction gun. The aim of this study is to discuss the air suction gun from the point of view of fluid mechanics and to propose useful information for designing the air suction gun with high suction performance using low energy.

2. Experiment

Figure 2 shows the outline of the experimental apparatus. The compressed air in a compressor ① was regulated to a set air pressure by a pressure adjuster ②, passed through a valve ③ and a flow meter ④, and arrived at a rectification tank ⑤. The air rectified in the rectification tank was supplied to an air suction gun ⑦ and flowed out to the atmosphere with a yarn. The tension and the speed of the yarn ⑧ released from a pirn ⑧ were regulated by a tension adjuster ⑨ and a speed adjuster (feed roller) ⑩ and then, the yarn was sucked into the air suction gun. Then, the yarn suction force was measured by a tension meter ⑪ and these data were saved to a computer ⑫.

Figure 3 shows the illustration of the air suction gun used in this study. The inner diameter of the yarn inhalation tube ① is 6 mm. The inner diameter of the four compressed-air inflow tubes ② is 2 mm, their axes and the axis of the de Laval tube ③ are not on the same plane, and the distance of the axes is 6.5 (=13/2) mm. The entrance and exit of the de Laval tube with a parallel part of 2 mm long are 15 mm in diameter. The inner diameter of the straight tube ④ is 20 mm. The focused geometry parameters of the air suction gun are 1) compressed-air inflow angle of nozzle ϕ, 2) passage diverging angle of nozzle θ, 3) throat diameter of the de Laval tube D, 4) converging angle of the de Laval tube α, and 5) the yarn propulsion tube length L composed of the de Laval tube and the straight tube. The values of each geometry parameter are shown in Table 1. Other experimental conditions were the running yarn speed v and the air pressure in the rectification tank p, which was called the supplied air pressure hereafter. We set up at the running yarn speed v = 600 m/min and the supplied air pressure p = 0.5 MPa (gauge pressure) in each experiment to measure the yarn suction force and the mass flow rate for clarifying geometry effects. Tested yarn used in this experiment was polyester multi-filament yarn of 167.7 dtex/48 f.

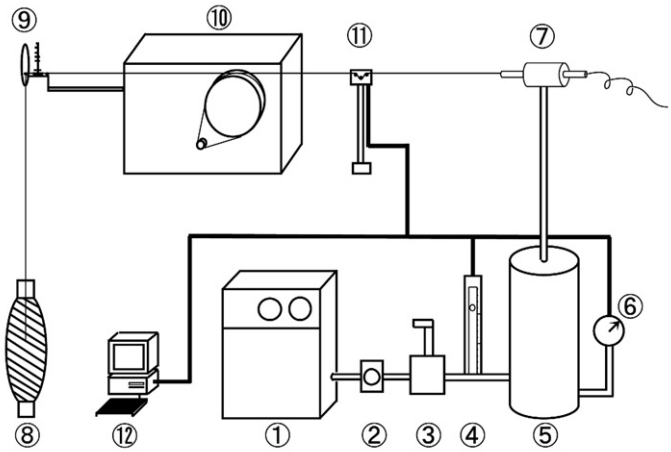

Fig. 2 Outline of the experimental apparatus.

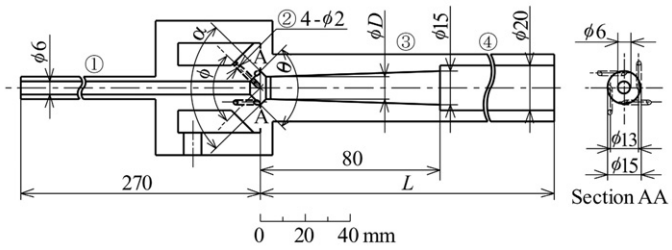

① yarn inhalation tube
② four compressed-air inflow tubes
③ de Laval tube
④ straight tube

Fig. 3 Illustration of the air suction gun used in this study (Yarn propulsion tube is composed of de Laval tube ③ and straight tube ④).

Table 1 Geometry parameters of the air suction gun.

Geometry parameter	Values
Compressed-air inflow angle of nozzle ϕ	60, 90, 120, 150, 165 °
Passage diverging angle of nozzle θ	30, 60, 90, 120 °
Throat diameter of de Laval tube D	9, 10, 11, 12, 13, 14 mm
Converging angle of de Laval tube α	30, 60, 90, 120, 150 °
Yarn propulsion tube length L	80, 200, 300, 400, 600, 800 mm

3. Results and discussions

3. 1 Time dependency of yarn suction force

Since the yarn suction force F showed oscillation against a passage of time t, its mean value F_m was discussed. When we advanced the experiments, we found two types of time dependency of F under some of experimental conditions.

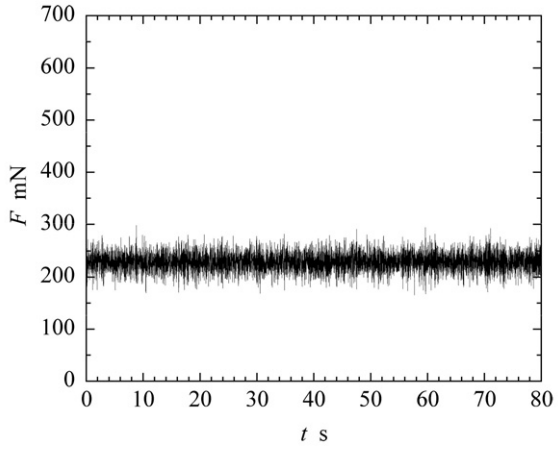

(a) Case 1 : small suction force

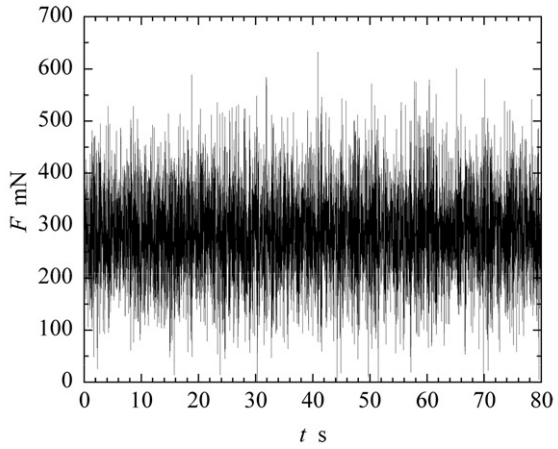

(b) Case 2 : large suction force

Fig. 4 Yarn suction force F as a function of measuring time t at the same experimental conditions of $\phi = 150°$, $\theta = 90°$, $D =$ 10 mm, $\alpha = 90°$, $L = 300$ mm, $v = 600$ m/min and $p = 0.5$ MPa.

Figure 4 shows an example of the time dependency of F under the same experimental conditions. The mean and amplitude of F shown in Fig. 4(a) are much different from those shown in Fig. 4(b). The case of small F is called Case 1 and the case of large F is called Case 2. The mean yarn suction force $F_m = 228.8$ mN and the standard deviation $F_s =$ 17.5 mN in the Case 1 and $F_m = 285.4$ mN, $F_s = 84.8$ mN in the Case 2. The mean yarn suction force F_m in the Case 2 is about 25 % larger than that in the Case 1.

The different time dependency of F under the same experimental condition appeared in the yarn after passing through the air suction gun. Figure 5 shows the photographs of the yarn appearance after passing through the air suction gun under the same experimental conditions. Figures 5(a) and 5(b) correspond to Figs. 4(a) and 4(b), respectively. In the Case 2 of the large mean and amplitude of F as shown in Fig. 4(b), knots appeared in the yarn after passing through the air suction gun. These knots did not appear in the Case 1 of the small yarn suction force.

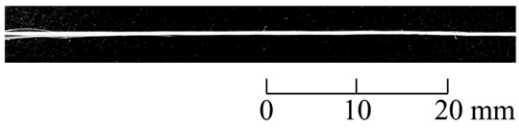

(a) Case 1 : small suction force

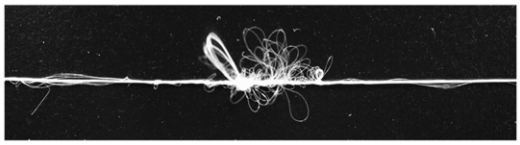

(b) Case 2 : large suction force

Fig. 5 Photographs of the yarn appearance after passing through the air suction gun at the same experimental conditions of $\phi = 150°$, $\theta = 90°$, $D = 10$ mm, $\alpha = 90°$, $L = 300$ mm, $v =$ 600 m/min and $p = 0.5$ MPa.

This phenomenon shown in the Case 2 frequently occurred in the case of large compressed-air inflow angle ϕ although the frequency of this occurrence depends on the geometry of the air suction gun and the experimental conditions. The jet angle of a compressed air is more vertical to the yarn axis at larger compressed-air inflow angle ϕ. In this case, the yarn is easier to be entangled, and then the knots are more easily formed in the yarn after passing through the air suction gun. As a result, the large yarn suction force occurs because of the large pressure drag in addition to the frictional drag in the yarn running direction when the knots are formed in the running yarn. In addition, the dispersion of the yarn suction force becomes large because the knots are not regularly and continuously formed in the running yarn and the airflow is very unsteady.

When F shows the two types of time dependency, we will use hereafter the smaller value of the Case 1 because the yarn suction characteristics of an air suction gun is represented by the smaller value.

3. 2 Geometry effects of air suction gun

Next, we will consider the geometry effects of an air suction gun on the yarn suction characteristics. In this section, we will discuss the effect of the geometry parameters of the air suction gun on the mean yarn suction force F_m and the air mass flow rate G. The operating conditions in the experiments were fixed at the yarn speed $v =$ 600 m/min and the supplied air pressure in the rectification tank $p = 0.5$ MPa (gauge pressure).

When we advanced the experiments to obtain the optimum values of the five geometry parameters, a long yarn propulsion tube length was expected to be desirable because the contact area between a running yarn and a high-speed air in the yarn propulsion tube is wide and the yarn

suction force is large. However, compactness of an air suction gun is also important because it is operated by a hand. Therefore, firstly we set the yarn propulsion tube length L = 300 mm although the total length of the gun was 570 mm.

To determine the optimum values of the four remaining parameters, a lot of experiments were carried out at a yarn propulsion tube length L of 300 mm. As a result, we obtained the compressed-air inflow angle ϕ = 150°, the passage diverging angle θ = 60°, the throat diameter of the de Laval tube D = 10 mm, and the converging angle of the de Laval tube α = 90°.

All of experimental data are impossible to be inserted here. As an example, Fig. 6 shows isoplethic lines of the mean yarn suction force F_m and the air mass flow rate G as a function of the compressed-air inflow angle ϕ and the passage diverging angle θ. Other experimental conditions are the throat diameter of the de Laval tube D = 10 mm, the converging angle of the de Laval tube α = 90°, and the yarn propulsion tube length L = 300 mm. When θ is fixed, F_m increases with an increment in ϕ and takes the maximum at ϕ = 150°. Since an air flows with a circumferential component as well as an axial one of the yarn propulsion tube, a yarn also may spirally run. Hence, as ϕ is large, the spiral pitch of the airflow becomes small, the yarn length in the yarn propulsion tube becomes long, frictional force between air

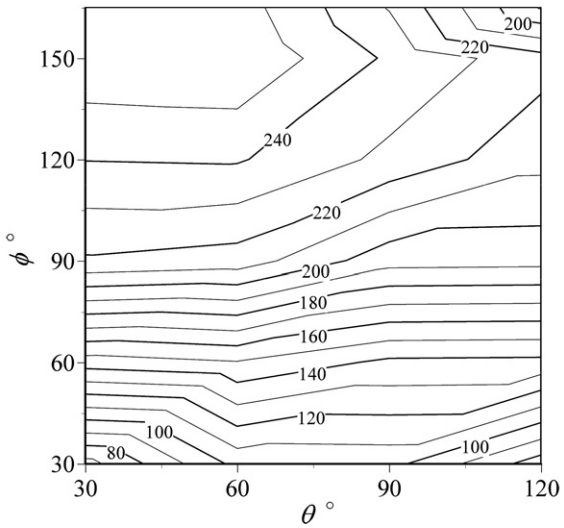

(a) Mean yarn suction force F_m [mN]

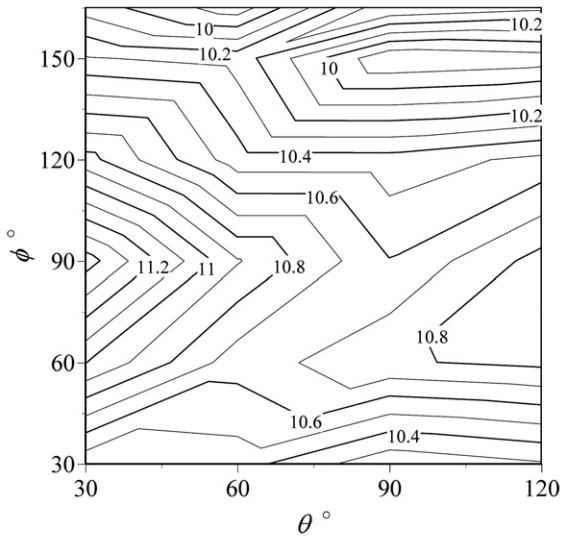

(b) Air mass flow rate G [g/s]

Fig. 6 Effect of the compressed-air inflow angle ϕ and the passage diverging angle θ on the characteristics of the air suction gun at D = 10 mm, α = 90°, L = 300 mm, v = 600 m/min and p = 0.5 MPa.

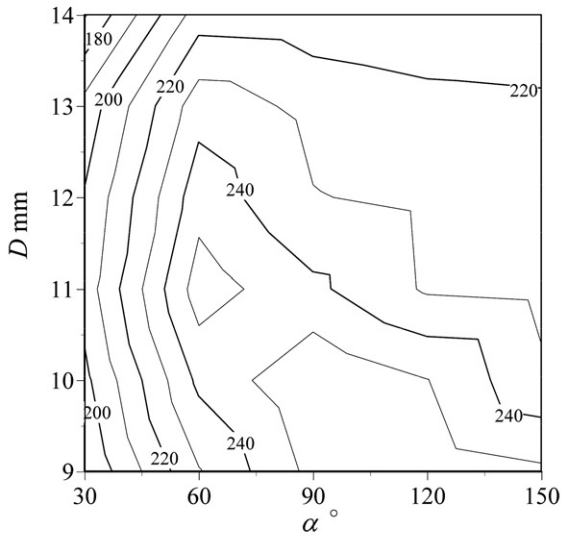

(a) Mean yarn suction force F_m [mN]

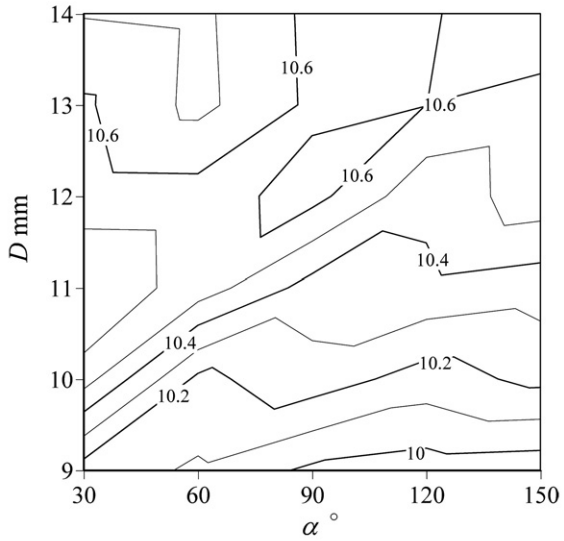

(b) Air mass flow rate G [g/s]

Fig. 7 Effect of the throat diameter of the de Laval tube D and the converging angle of the de Laval tube α on the characteristics of the air suction gun at ϕ = 150°, θ = 60°, L = 300 mm, v = 600 m/min and p = 0.5 MPa.

and yarn becomes large, and then, F_m becomes large. For too large ϕ such as 165°, however, the circumferential component of airflow is too large and then the propulsion is small. When ϕ is fixed, F_m shows a tendency that it takes the maximum in $\theta = 60 \sim 90°$ in the case of small ϕ of 30°, it is independent of θ in the case of $\phi = 60 \sim 90°$, and it decreases with an increase in θ in the case of ϕ greater than 90°. However, the dependency of F_m on θ is much smaller than that on ϕ. G is nearly constant although it seems to be the maximum near $\phi = 90°$.

As another example, Fig. 7 shows isoplethic lines of the mean yarn suction force F_m and the air mass flow rate G as a function of the throat diameter of the de Laval tube D and the converging angle of the de Laval tube α. Other experimental conditions are the compressed-air inflow angle $\phi = 150°$, the passage diverging angle $\theta = 60°$, and the yarn propulsion tube length L = 300 mm. When α is fixed, F_m is the maximum near D = 10 mm. When D is fixed, F_m shows the maximum in $\alpha = 60 \sim 90°$. When α is fixed, G increases with an increment in D because of an increment of the cross-sectional area of flow region. The air mass flow rate G does not show a large dependency on α although it shows a little decrease with an increase in α. On the whole, G seems to be the maximum near $\alpha = 90°$. The dependency of G on α is smaller than that on D.

In order to discuss the optimum geometry of the air suction gun from the point of view of energy, we defined the yarn suction efficiency η as the mean yarn suction force F_m divided by the air mass flow rate G and evaluated the characteristics of the yarn suction gun. The air mass flow rate G has a positive correlation with the consumption of electricity. Therefore, the air suction gun with high η is highly efficient from the point of view of energy. Figures 8 and 9 show isoplethic lines of the yarn suction efficiency η obtained from the data of Figs. 6 and 7.

Figure 8 shows the effect of the compressed-air inflow angle ϕ and the passage diverging angle θ on the yarn suction efficiency η. When θ is fixed, η increases with an increment in ϕ and takes the maximum at $\phi = 150°$. When ϕ is fixed, η takes the maximum near $\theta = 60°$ except in the case of small ϕ such as 30°. As a result, the optimum geometries of an air suction gun are $\phi = 150°$ and $\theta = 60°$ from the point of view of energy efficiency.

Figure 9 shows the effect of the throat diameter of the de Laval tube D and the converging angle of the de Laval tube α on the yarn suction efficiency η. When α is fixed, η takes the maximum near D = 11 mm for small α and near D = 10 mm for $\alpha > 75°$. When D is fixed, η takes the maximum in $\alpha = 60 \sim 90°$ and decreases a little with an increase in α for large α. As a result, the optimum geometries of an air suction gun are D = 10 mm and $\alpha = 90°$ from the point of view of energy efficiency.

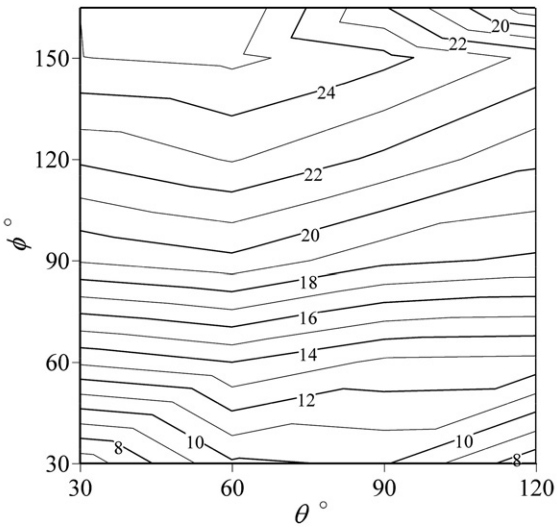

Fig. 8 Effect of the compressed-air inflow angle ϕ and the passage diverging angle θ on the yarn suction efficiency η [N/(kg/s)] at D = 10 mm, $\alpha = 90°$, L = 300 mm, v = 600 m/min and p = 0.5 MPa.

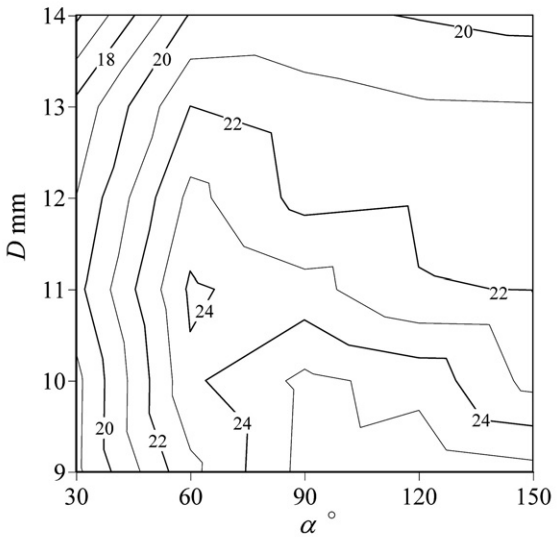

Fig. 9 Effect of the throat diameter of the de Laval tube D and the converging angle of the de Laval tube α on the yarn suction efficiency η [N/(kg/s)] at $\phi = 150°$, $\theta = 60°$, L = 300 mm, v = 600 m/min and p = 0.5 MPa.

From Figs. 6 ~ 9, since G is hardly affected by the geometry of the air suction gun compared with F_m, η shows a distribution similar to F_m. This implies that it is possible to predict the tendency of η by using the measurement data of F_m.

We obtained the compressed-air inflow angle $\phi = 150°$, the passage diverging angle $\theta = 60°$, the throat diameter of the de Laval tube D = 10 mm and the converging angle of the de Laval tube $\alpha = 90°$ at the yarn propulsion tube length L = 300 mm. Finally we will discuss the effect of the yarn propulsion tube length L on the yarn suction efficiency η.

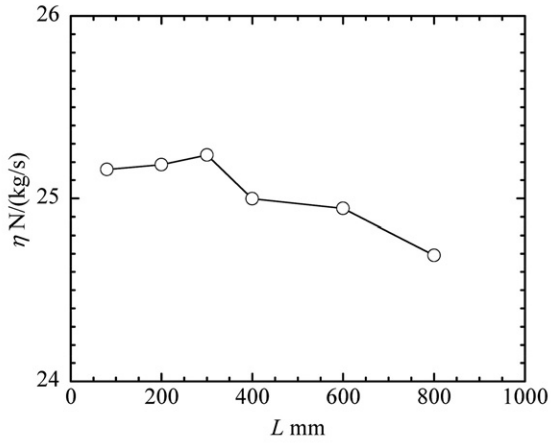

Fig. 10 Yarn suction efficiency η as a function of the yarn propulsion tube length L at $\phi = 150°$, $\theta = 60°$, $D = 10$ mm, $\alpha = 90°$, $v = 600$ m/min and $p = 0.5$ MPa.

Figure 10 shows η as a function of L. The operating conditions in this experiment are the running yarn speed $v = 600$ m/min and the supplied air pressure in the rectification tank $p = 0.5$ MPa. The dependency of η on L is comparatively small. Detail consideration of the effect of L on η should be a future research topic.

3. 3 Proposal and evaluation of air suction gun with high energy efficiency

The geometry of the nozzle, the de Laval tube and the yarn propulsion tube constituting an air suction gun with high yarn suction efficiency was made clear from these experimental results. Table 2 shows the geometry of our proposing air suction gun with high yarn suction efficiency.

Figures 11 and 12 show the mean yarn suction force F_m and the yarn suction efficiency η of our proposing air suction gun as a function of the running yarn speed v at the supplied air pressures in the rectification tank p = 0.4, 0.5 and 0.6 MPa. As shown in Fig. 11, when p is fixed, F_m decreases with an increase in v because when the relative velocity of running yarn to air velocity is small, frictional force is small. When p is high, F_m is large because of large air mass flow rate. As shown in Fig. 12, η shows similar

Table 2 Geometry of the high efficiency air suction gun. See Fig. 3 about detailed information on the geometry parameters.

Geometry parameter	Value
Compressed-air inflow angle of nozzle ϕ	150 °
Passage diverging angle of nozzle θ	60 °
Throat diameter of de Laval tube D	10 mm
Converging angle of de Laval tube α	90 °
Yarn propulsion tube length L	300 mm

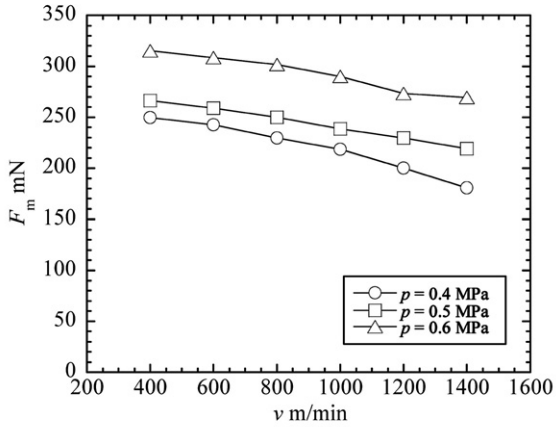

Fig. 11 Mean yarn suction force F_m as a function of the yarn speed v at $\phi = 150°$, $\theta = 60°$, $D = 10$ mm, $\alpha = 90°$, $L = 300$ mm, and $p = 0.4$, 0.5 and 0.6 MPa.

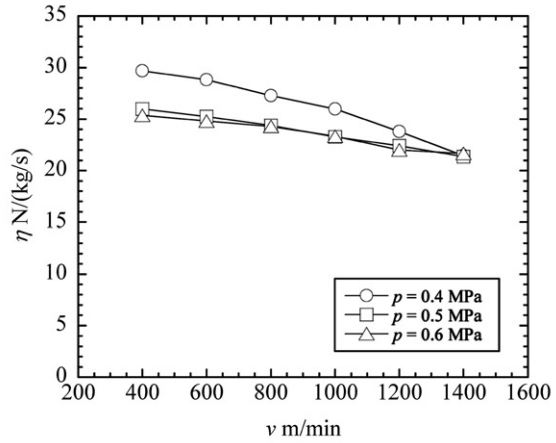

Fig. 12 Yarn suction efficiency η as a function of the yarn speed v at $\phi = 150°$, $\theta = 60°$, $D = 10$ mm, $\alpha = 90°$, $L = 300$ mm, and $p = 0.4$, 0.5 and 0.6 MPa.

variation to F_m against v. However, η in small v is higher at smaller p, and the dependency of η on p decreases with an increase in v and vanishes completely at $v = 1400$ m/min.

4. Conclusions

We experimentally discussed the geometry effect of an air suction gun on the characteristics of suction of running yarn. Our focusing parameters are 1) Compressed-air inflow angle of nozzle ϕ, 2) Passage diverging angle of nozzle θ, 3) Throat diameter of the de Laval tube D, 4) Converging angle of the de Laval tube α and 5) Yarn propulsion tube length L. Results obtained are as follows:

(1) Yarn suction efficiency, defined as the mean yarn suction force divided by the mass flow rate of compressed-air, strongly depends on the compressed-air inflow angle ϕ and the converging angle of the de Laval tube α. On the contrary, it is almost independent of the passage diverging angle θ and the throat diameter of the de Laval tube D. We

were able to obtain the optimum geometry of the air suction gun from the point of view of energy efficiency.
(2) There are two types of time dependency of the yarn motion and suction force even under the same experimental conditions.

References

[1] Iemoto Y, Chono S, Sawazaki K (1989) J Text Mach Soc Japan (predecessor journal of J Text Eng), **35**(1), 1–5

[2] Iemoto Y, Chono S, Sawazaki K (1989) J Text Mach Soc Japan (predecessor journal of J Text Eng), **35**(3), 1–5

[3] Iemoto Y, Chono S (1997) J Text Mach Soc Japan (predecessor journal of J Text Eng), **43**, 38–46

[4] Iemoto Y, Chono S, Tanaka T (1998) J Text Mach Soc Japan (predecessor journal of J Text Eng), **44**, 57–63

[5] Iemoto Y, Chono S, Terachi T (1999) J Text Mach Soc Japan (predecessor journal of J Text Eng), **45**, 36–43

[6] Iemoto Y, Chono S, Tanaka T (1999) J Text Mach Soc Japan (predecessor journal of J Text Eng), **45**, 44–50

[7] Iemoto Y, Chono S, Kasamatsu K, Lou W (1999) J Text Mach Soc Japan (predecessor journal of J Text Eng), **45**, 71–77

[8] Chono S, Iemoto Y (1999) J Text Mach Soc Japan (predecessor journal of J Text Eng), **45**, 108–112

[9] Iemoto T, Chono S, Qin H, Lou W (2000) J Text Eng, **46**, 11–19

[10] Lou W, Iemoto Y, Chono S (2000) J Text Eng, **46**, 53–61

[11] Iemoto Y (1997) Japanese J Multiphase Flow, **11**, 23–29

[12] Murakami K, Tokunaga K, Nomura S, Naito S, Abe M (2006) J Text Eng, **52**, 73–79

[13] Tokunaga K, Murakami K, Kitamura M, Nomura S, Naito S (2006) J Text Eng, **52**, 121–129

[14] Qiu H, Iemoto Y, Tanoue S (2007) J Text Eng, **53**, 1–8

[15] Qiu H, Iemoto Y, Tanoue S (2007) J Text Eng, **53**, 59–67

[16] Shintani R, Shintaku S, Okajima A (2000) J Text Mach Soc Japan (predecessor journal of J Text Eng), **53**, T217–T224

[17] Shintani R, Okajima A (2001) J Text Mach Soc Japan (predecessor journal of J Text Eng), **54**, T9–T16

[18] Shintani R, Okajima A (2002) J Text Mach Soc Japan (predecessor journal of J Text Eng), **55**, T59–T64

[19] Shintani R, Okajima A (2002) J Text Mach Soc Japan (predecessor journal of J Text Eng), **55**, T73–T81